Time-lapse full-waveform inversion for ocean-bottom node seismic data with seawater velocity changes

Xin Fu and Kris Innanen

ABSTRACT

As a powerful tool for 4D seismic data inversion to monitor subsurface reservoir changes and/or CO_2 storages, full waveform inversion (FWI) has the ability of high-resolution imaging of physical properties for subsurface media, and it can solve the problem of non-repeatable receiver/source positions in time-lapse seismic surveys. In this report, we develop a three-stage time-lapse FWI strategy for ocean-bottom node seismic data, in which the first stage is to use FWI to estimate the seawater velocities in the baseline model and the monitor model, respectively; the second stage is to obtain a relatively good common starting model that is close to the final inversion result, to guide the next baseline FWI and monitor FWI to converge to local minima that are closing to each other; the third stage is to employ the better starting models acquired in the second stage to carry out the final convergence and reflect the time-lapse differences. The tests using synthetic data obtained from acoustic models with different levels of seawater velocity changes have demonstrated the feasibility and stability of our new method.

INTRODUCTION

Applying time-lapse (4D) seismic methods for reservoir monitoring and characterization has developed for a long time since the mid-late 1980s (Greaves and Fulp, 1987; Lumley, 2001; Landrø, 2001; Calvert, 2005; Hicks et al., 2016; Jack, 2017; Cho and Jun, 2021), which can be employed to monitor reservoir changes caused by the production of hydrocarbon (e.g., enhanced oil recovery) and the unground storage of CO_2. Especially, due to the increasing demand for technologies to control greenhouse gas emissions, storing CO_2 in the subsurface has been being developing by many researchers, and 4D seismic methods are used to monitor the CO_2 storages accordingly (Egorov et al., 2017; Cho and Jun, 2021; Ajo-Franklin et al., 2013; Macquet et al., 2019). However, successful seismic monitoring depends on the repeatability between baseline and monitor surveys that can be affected by variations in weather conditions, source and receiver positions, environmental noises, source wavelets, seawater or near-surface properties, etc.

The impact of the variations can be alleviated by good acquisition plans and/or proper processing, e.g., repeatable acquisition geometries and data processing procedures. To obtain good repeatable data to monitor the reservoir changes, the permanent OBC (ocean-bottom-cable) installations are set at Foinhaven and Valhall fields (Calvert, 2005; Yang et al., 2016). And at the Aneth oil field in Utah, the receivers are cemented in the monitor well to acquire time-lapse VSP (vertical seismic profile) data (Cheng et al., 2010). In the CO2CRC Otway field experiment, Shulakova et al. (2015) improve the repeatability of the land seismic data by burying the receivers which can lower the noises caused by poor weather conditions, non-repeatable receiver positions, near-surface changes, and non-repeatable survey environments. During the data processing, a cross-equalization method is often applied to enhance the repeatability between baseline and monitor data (Rickett and Lumley, 2001). Fu et al. (2020) propose a double-wavelet method to eliminate the source wavelet non-repeatability which can also be reduced by designing a matching filter (Fu and Innanen, 2022c). In past years, time-lapse seismic surveys based on a fiber-optic distributed acoustic sensing (DAS) system becomes increasingly popular, since the down-hole DAS array can be permanently installed, has lower monitoring cost, and is of finer spatial sampling (Zwartjes et al., 2018; Byerley et al., 2018; Wilson et al., 2021).

As a powerful tool for 4D seismic data inversion to monitor subsurface reservoir changes and/or CO_2 storages, full waveform inversion (FWI) (Lailly et al., 1983; Tarantola, 1984; Virieux and Operto, 2009) has the ability of high-resolution imaging of physical properties for subsurface media, and it can solve the problem of non-repeatable receiver/source positions in time-lapse seismic surveys (Zhou and Lumley, 2021b). In the past decade, many time-lapse FWI methods have been developed. The most conventional time-lapse FWI strategy is the parallel strategy (Lumley et al., 2003; Plessix et al., 2010), but its result is prone to be affected by the convergence difference (Yang et al., 2015) and non-repeatable receiver/source positions (Zhou and Lumley, 2021b; Fu and Innanen, 2022a) between baseline and monitor inversion. Routh et al. (2012) present the sequential strategy, using the inverted baseline model as a starting model for monitor inversion, which can help to save computational cost and has been justified in a field VSP data case (Egorov et al., 2017). However, this strategy often generates strong artifacts since it enhances the convergence difference between twice FWIes (Yang et al., 2015; Zhou and Lumley, 2021b). But a local-updating sequential strategy can efficiently reduce the artifacts and perform well in both synthetic and field time-lapse data (Raknes and Arntsen, 2014; Asnaashari et al., 2015). Also, the local-updating method can be incorporated with the double-difference strategy, which will be introduced later, to improve the time-lapse results (Zhang and Huang, 2013; Li et al., 2021), alleviate the impact of taking an acoustic approximation to elastic subsurface rocks (Willemsen et al., 2016), or implement Bayesian/Markov Chain Monte Carlo formulation of time-lapse FWI (Fu and Innanen, 2022b). And the local-solver-based local-updating method can significantly decrease the computational cost of time-lapse FWI (Willemsen, 2017; Huang et al., 2018; Kotsi et al., 2020). Of course, the local-updating method needs prior location information about reservoir change, which may be not easy to be obtained in some cases of non-repeatable time-lapse surveys, such as the ones in this study.

The double-difference strategy, directly minimizing residuals between synthetic difference data (synthetic monitor data minus synthetic baseline data) and observed difference data (observed monitor data minus observed baseline data), applied in 4D FWI first by Zheng et al. (2011), has been adopted by several researchers (Zhang and Huang, 2013; Raknes and Arntsen, 2014; Yang et al., 2015; Willemsen et al., 2016; Fu and Innanen, 2021) including a real data case in Yang et al. (2016). It can focus on reservoir changes and reduce artifacts outside the reservoir, hence, its result is not sensitive to the convergence degree of the inverted baseline model. Nevertheless, the double-difference strategy requires well repeated time-lapse surveys. Fu et al. (2020) introduce a double-wavelet method to handle the case of non-repeatable baseline and monitor source wavelets. But the double-difference strategy is still vulnerable to the non-repeatability of receiver/source positions. The common-model strategy, presented by Hicks et al. (2016), can also decay the artifacts caused by the divergence difference between baseline and monitor inversions (Fu and Innanen, 2022a). Its philosophy is employing the same relatively well-converged starting model for baseline and monitor FWIes to guide them into the same local minimum, and it has been applied in field cases in Hicks et al. (2016) and Bortoni et al. (2021). Moreover, Maharramov et al. (2016) present a joint method in which baseline and monitor models are simultaneously inverted; Zhou and Lumley (2021a) propose a central-difference strategy containing two sequential strategies; and Fu and Innanen (2022a) build a stepsize-sharing strategy by sharing stepsizes between baseline and monitor inversions, which can eliminate the artifacts linked to the convergence difference and is suitable when the starting model is biased. However, in all the methods mentioned above, none has been demonstrated that it has the property of solving the non-repeatability issues of seawater or near-surface velocity changes between time-lapse seismic surveys.

In this paper, we will develop a new time-lapse FWI strategy for OBN (ocean-bottom node), to alleviate the impact of seawater velocity changes on time-lapse inversions. The synthetic seismic data obtained from acoustic models with different levels of seawater velocity changes will be used to perform our new method.

TIME-LAPSE FWI METHODS

Full-waveform inversion

A standard FWI (Lailly et al., 1983; Tarantola, 1984; Virieux and Operto, 2009) is minimizing the L2 norm misfit function:

$$E(\mathbf{m}) = \frac{1}{2}||\mathbf{d}_{obs} - \mathbf{F}(\mathbf{m})||_2^2, \tag{1}$$

where $\mathbf{d}_{obs}$ is the observed data or recorded wavefields, $\mathbf{F}(\cdot)$ is a forward modeling operator based on the wave equation, and $\mathbf{m}$ is the updating model (e.g., P-wave velocity).

By a linearized optimization (e,g, steepest descent method, conjugate gradient method, etc.), the model is updated iteratively as:

$$\mathbf{m}^k = \mathbf{m}^{k-1} + \delta\mathbf{m}^k, \tag{2}$$

where k is the iteration number, and

$$\delta\mathbf{m}^k = \mu^k \mathbf{g}(\mathbf{m}^{k-1}, \mathbf{d}_{res}^{k-1}), \tag{3}$$

where

$$\mathbf{d}_{res}^{k-1} = \mathbf{d}_{obs} - \mathbf{F}(\mathbf{m}^{k-1}), \tag{4}$$

in which $\mathbf{g}(\mathbf{m}^{k-1}, \mathbf{d}_{res}^{k-1})$ is the updating direction of model in iteration k, which depends on the updated model $\mathbf{m}^{k-1}$ and data residual $\mathbf{d}_{res}^{k-1}$ in iteration $k-1$. For different optimizations, it has different calculations, for instance, in the steepest descent method, $\mathbf{g}$ represents the gradient of the misfit function (equation 1) with respect to $\mathbf{m}$, which is the zero-lag cross-correlation between forward wavefileds and backward wavefields of data residuals. For the first iteration, a starting model $\mathbf{m}^0$ have to be prepared, which can be obtained by velocity analysis or tomography.

In this study, we will typically use a time-domian constant-density acoustic finite-difference method as the forward modeling operator, the steepest descent method as the optimization, and the gradient is preconditioned with the diagonal approximation of the Hessian matrix (Shin et al., 2001).

Tested time-lapse inversion strategies

In the introduction section, we have introduced the parallel strategy, the sequential strategy, the double-difference strategy, the common-model strategy, the central-difference strategy, the stepsize-sharing strategy, and the joint method. Exhaustively testing all the methods is too resource-intensive. Hence, in this study, we only test the three typical strategies (the parallel strategy, the sequential strategy, and the double-difference strategy), and the common-model strategy that has been applied in a case with minor seawater velocity changes in Hicks et al. (2016).

Parallel strategy

As the most conventional time-lapse inversion strategy, the parallel strategy, , with workflow illustrated in Figure 1a, includes two independent FWI processes. One is for baseline model inversion, and inputs are the baseline data and a starting model. Another one is for monitor model inversion, and inputs are the monitor data and the same starting model as that in the baseline model inversion. Then the inverted time-lapse model is the inverted monitor model subtract the inverted baseline model. Since FWI is highly non-linear and is easy to be stuck in different minima, the two FWI processes mentioned above often have different convergences and yield many artifacts on the final time-lapse inversion.

Sequential strategy

The sequential strategy, with workflow illustrated in Figure 1b, has the same baseline model inversion as the PRS, using baseline data and a starting model to obtain the baseline model. But the second time inversion, monitor model inversion, is different, in which the inverted baseline model is sequentially employed as the starting model for the monitor model inversion. Then the inverted monitor model minus the inverted baseline model is the time-lapse model.

Double-difference strategy

The double-difference strategy, with workflow illustrated in Figure 1c, also contains twice FWI processes. This first one is still the baseline model inversion, the same as that in the parallel strategy or sequential strategy. In the second monitor model inversion, the starting model is the inverted baseline model, same as the sequential strategy, but the input monitor data are not the observed monitor data which are altered to the composited data:

$$\mathbf{d}_{DD} = \mathbf{F}(\mathbf{m}_{bas}) + (\mathbf{d}_{mon} - \mathbf{d}_{bas}), \tag{5}$$

where $\mathbf{F}(\mathbf{m}_{bas})$ is the synthetic data of inverted baseline model $\mathbf{m}_{bas}$, $(\mathbf{d}_{mon} - \mathbf{d}_{bas})$ is the difference data (observed monitor data $\mathbf{d}_{mon}$ subtract observed baseline data $\mathbf{d}_{bas}$). Ac-

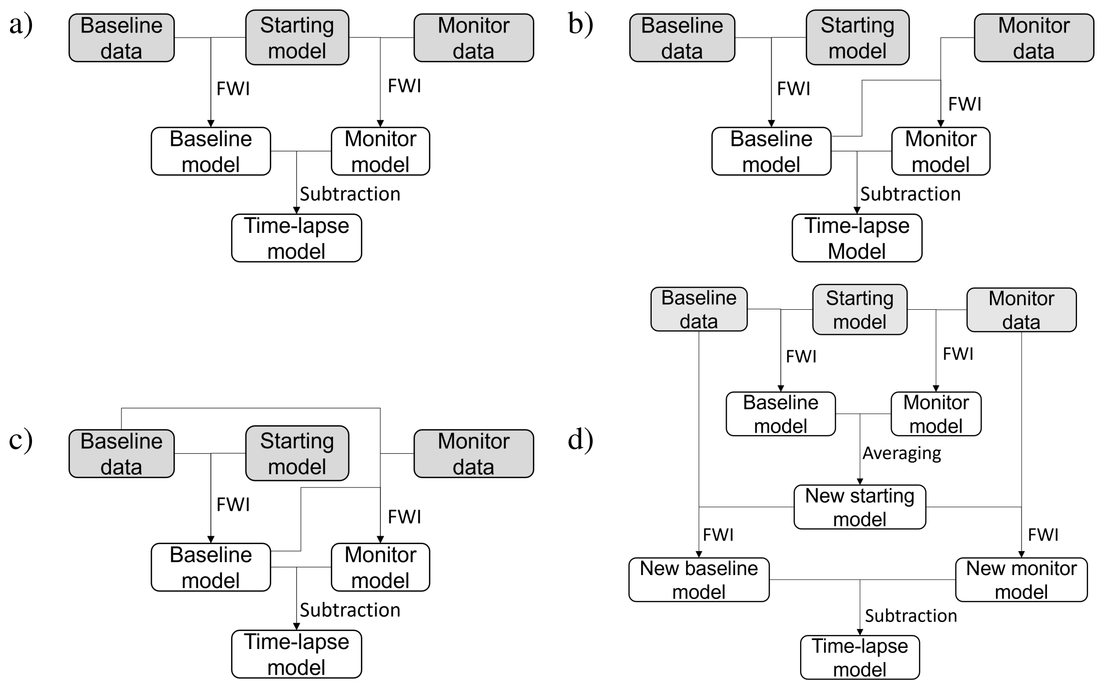

FIG. 1. Workflows of (a) the parallel strategy, (b) the sequential strategy, (c) the double-difference strategy, and (d) the common-model strategy.

cordingly, the misfit function for monitor model inversion becomes:

$$\mathbf{E}_{DD}(\mathbf{m}_{mon}) = \frac{1}{2}||\mathbf{d}_{DD} - \mathbf{F}(\mathbf{m}_{mon})||_2^2, \tag{6}$$

where $\mathbf{F}(\mathbf{m}_{mon})$ is the synthetic data of inverted monitor model $\mathbf{m}_{mon}$.

Common-model strategy

The common-model strategy, with workflow illustrated in Figure 1d, can be seen as an upgraded version of the strategy. Essentially, it contains twice parallel strategies. Firstly, the baseline and monitor model inversions are performed independently with the same starting model. Then a new starting model is taken from the average of baseline and monitor models, with which the baseline and monitor model inversions are performed independently again, still using the original data sets. And the final time-lapse change is obtained from the difference of baseline and monitor models in the second-time parallel strategy.

Note that in the original version of the common-model strategy in Hicks et al. (2016), the first-time parallel strategy only uses low-frequency seismic components, and only high-frequency seismic components are employed in the second-time parallel strategy. It may cause a low-frequency component lack in the final inverted time-lapse change. Hence, we use all-frequency seismic components for every single FWI process to enhance the original version.

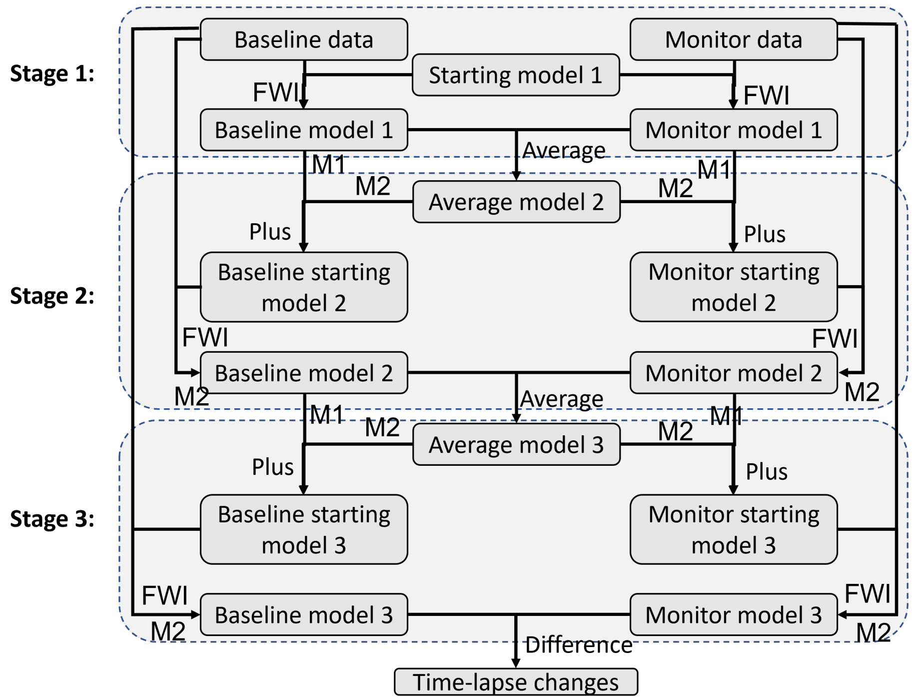

FIG. 2. The workflow of the three-stage time-lapse FWI strategy (TSS), in which $\mathbf{M1}$ and $\mathbf{M2}$ are weighting matrices plotted in Figure 3.

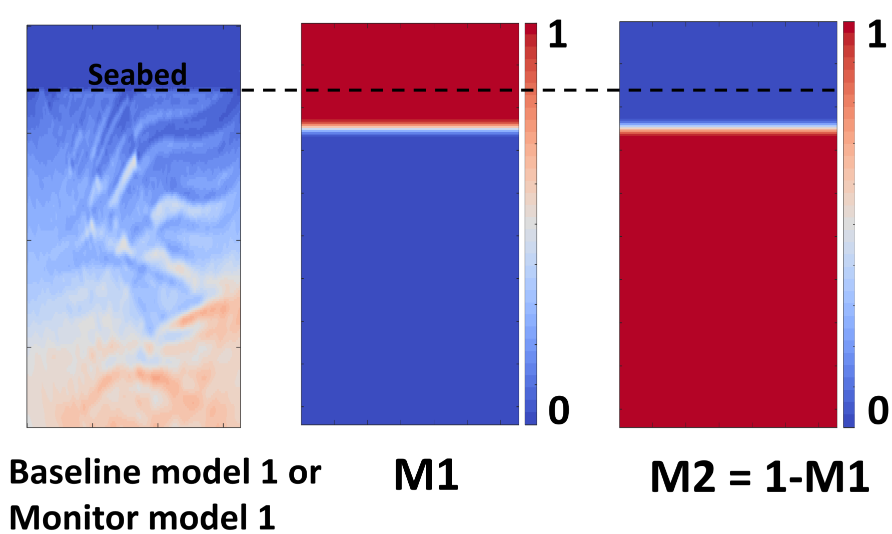

FIG. 3. Weighting matrices, $\mathbf{M1}$ and $\mathbf{M2}$ $(= 1 - \mathbf{M1})$, that are employed in Figure 2. The matrices are designed according to the seabed that can be located from the inverted baseline or monitor model (the first panel) obtained from stage 1 of the TSS. The tapers in $\mathbf{M1}$ and $\mathbf{M2}$ are slightly lower than the seabed.

A three-stage time-lapse inversion strategy

In this section, we propose a novel time-lapse FWI strategy to deal with the issue of non-repeatable seawater velocities. Zhou and Lumley (2021b) point out that utilizing accurate seawater velocities of baseline and monitor models can effectively decay artifacts caused by non-repeatable seawater velocities in the inverted time-lapse changes. Nevertheless, precise seawater velocities are nearly impossible to be obtained, which vary with seawater temperature, depth, and salinity of the seawater (Medwin, 1975). The seawater feature changes very locally. Fortunately, applying FWI of seismic data to estimate seawater velocities has been demonstrated as a feasible scheme **?**. On the other hand, the common-model strategy is much more stable than the double-difference strategy in the case of non-repeatable source/receiver positions, and it is more capable of suppressing artifacts caused by the convergence difference between baseline and monitor FWIes than the parallel strategy and the sequential strategy (Fu and Innanen, 2022a).

By incorporating thoughts of both the common-model strategy and the seawater velocity estimation using seismic FWI, we propose a novel time-lapse strategy, with workflow illustrated in Figure 2. It consists of the following steps:

1. Starting with the same starting model ($Starting\ model\ 1$) that can be built from velocity analysis or tomography, FWIes are performed independently on baseline data and monitor data. Therefore, we have obtained the first baseline model ($Baseline\ model\ 1$) and the first monitor model ($Monitor\ model\ 1$). Also, the seawater velocities have been estimated in the above two inverted models.

2. According to $Baseline\ Model\ 1$ or $Monitor\ Model\ 1$, two weighting matrices ($\mathbf{M1}$ and $\mathbf{M2}$) are designed. The two matrices are plotted in Figure 3, where you can see they both contain three areas: 0-value area, 1-value area, and a median area (or taper) smoothly switching from 0 to 1. And the median area is slightly deeper than the seabed that can be located from $Baseline\ model\ 1$ or $Monitor\ model\ 1$. $\mathbf{M1}$ is designed to extract the estimated seawater velocities and avoid precisely picking up the seabed. $\mathbf{M2}$ equals $1 - \mathbf{M1}$, is to prevent the estimated seawater velocities from being updated or changed. The smoothed median area can help to smoothly plant the estimated seawater velocities to the updated models in the next steps. $\mathbf{M1}$ is generated by smoothing a Heaviside step function.

3. Two new starting models ($Baseline\ starting\ model\ 2$ and $Monitor\ starting\ model\ 2$) are established. First, $Average\ model\ 2$ is calculated by averaging the inverted $Baseline\ Model\ 1$ and $Monitor\ Model\ 1$. Then, two new starting models, $Baseline\ starting\ model\ 2$ and $Monitor\ starting\ model\ 2$, are, respectively, computed by

$$Baseline\ starting\ model\ 2 = \mathbf{M1} \odot Baseline\ Model\ 1 + \mathbf{M2} \odot Average\ model\ 2, \tag{7}$$

and

$$Monitor\ starting\ model\ 2 = \mathbf{M1} \odot Monitor\ Model\ 1 + \mathbf{M2} \odot Average\ model\ 2, \tag{8}$$

where $\odot$ denotes the element-wise product.

4. The new baseline model ($Baseline\ model\ 2$) and new monitor model ($Monitor\ model\ 2$) are inverted by implementing baseline FWI and monitor FWI separately. The inputs for baseline FWI are $Baseline\ data$ and $Baseline\ starting\ model\ 2$, and inputs for monitor FWI are $Monitor\ data$ and $Monitor\ starting\ model\ 2$. Additionally, to preserve the estimated seawater velocities, the gradients $\mathbf{g}$ of misfit function $E(\mathbf{m})$ in both baseline and monitor inversions are multiplied with the weighting matrix $\mathbf{M2}$.

5. Another two new starting models ($Baseline\ starting\ model\ 3$ and $Monitor\ starting\ model\ 3$) are calculated. $Average\ model\ 3$ is calculated from $Baseline\ Model\ 2$ and $Monitor\ Model\ 2$ first. And then, $Baseline\ starting\ model\ 3$ and $Monitor\ starting\ model\ 3$ are computed by

$$Baseline\ starting\ model\ 3 = \mathbf{M1} \odot Baseline\ Model\ 2 + \mathbf{M2} \odot Average\ model\ 3, \tag{9}$$

   and

$$Monitor\ starting\ model\ 3 = \mathbf{M1} \odot Monitor\ Model\ 2 + \mathbf{M2} \odot Average\ model\ 3. \tag{10}$$

6. Again, the final inverted baseline model ($Baseline\ model\ 3$) and monitor model ($Monitor\ model\ 3$) are obtained by performing baseline and monitor FWIes independently. The inputs for baseline FWI are $Baseline\ data$ and $Baseline\ starting\ model\ 3$, and inputs for monitor FWI are $Monitor\ data$ and $Monitor\ starting\ model\ 3$. And the estimated seawater velocities are still kept by multiplying the gradients of misfit functions with the weighting matrix $\mathbf{M2}$.

7. The final estimated time-lapse changes equals $Monitor\ model\ 3$ minus $Baseline\ model\ 3$.

The above steps can be summarized into three stages, as shown in Figure 2: the first stage is to use FWI to estimate the seawater velocities in the baseline model and the monitor model, respectively; the second stage is to obtain a relatively good common starting model that is close to the final inversion result, to guide the next baseline FWI and monitor FWI to converge to local minima that are closing to each other; the third stage is to employ the better starting models acquired in the second stage to carry out the final convergence and reflect the time-lapse differences. Since the proposed method includes three stages, we call it "the three-stage strategy (TSS)".

NUMERICAL EXAMPLES

In this section, we test the TSS with four different time-lapse models including model 1, model 2, mode 3, and model 4, and each model contains an identical baseline model (Figure 4a), and a different monitor model. Model 1 contains a monitor model that is of the time-lapse change 1 (monitor model minus baseline model, Figure 4c), with a $150m/s$ reservoir change at the below center but without any seawater velocity changes. Except for the same reservoir velocity change, in the monitor models of models 2, 3, and 4, there still are some seawater velocity changes added. The seawater velocity changes decrease

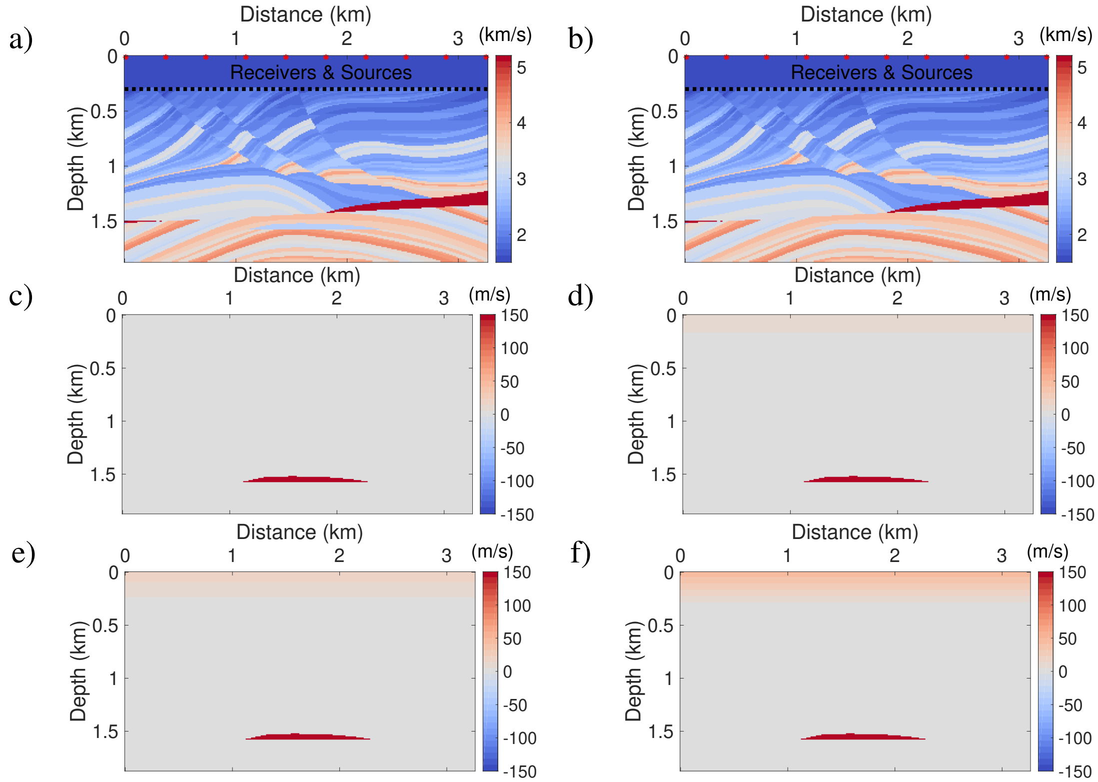

FIG. 4. (a) Baseline model. (b) Monitor model. (c) Time-lapse change 1 without seawater velocity change. (d) Time-lapse change 2, the maximum seawater velocity change is $10m/s$. (e) Time-lapse change 3, the maximum seawater velocity change is $20m/s$. (f) Time-lapse change 4, the maximum seawater velocity change is $50m/s$. The seawater velocity change is decreasing with depth.

with depth, the maximum seawater velocity changes in models 2, 3, and 4 are, respectively, $10m/s$, $20m/s$, and $50m/s$. And the time-lapse changes for models 1, 2, 3, and 4 are, respectively, plotted in Figure 4c-f.

In another report, we investigated the performance of the parallel strategy, the sequential strategy, the double-difference strategy, and the common model strategy using the four models mentioned above. It concluded that the double-difference strategy is the best one when the acquisition systems for baseline and monitor surveys are identical. Especially, only the double-difference strategy can provide a valuable result of the time-lapse changes for model 3. Hence, here we only perform the double-difference strategy, as a representative of the conventional time-lapse strategies, to have a comparison with the TSS. The inverted time-lapse changes of the double-difference strategy for models 1, 2, 3, and 4 are, respectively, plotted in Figure 5a-d. The baseline inversions of the three stages in the TSS are displayed in Figures 6a-c, 7a-c, and 8a-c, in which starting baseline models, the curves of baseline data misfits versus iteration numbers, and the inverted baseline models for three stages are plotted. From them, we can monitor the inversion quality of each stage. The inverted time-lapse changes of the TSS for models 1, 2, 3, and 4 are, respectively, plotted in Figure 9a-d. We observe that the TSS gives better results than the double-difference strategy.

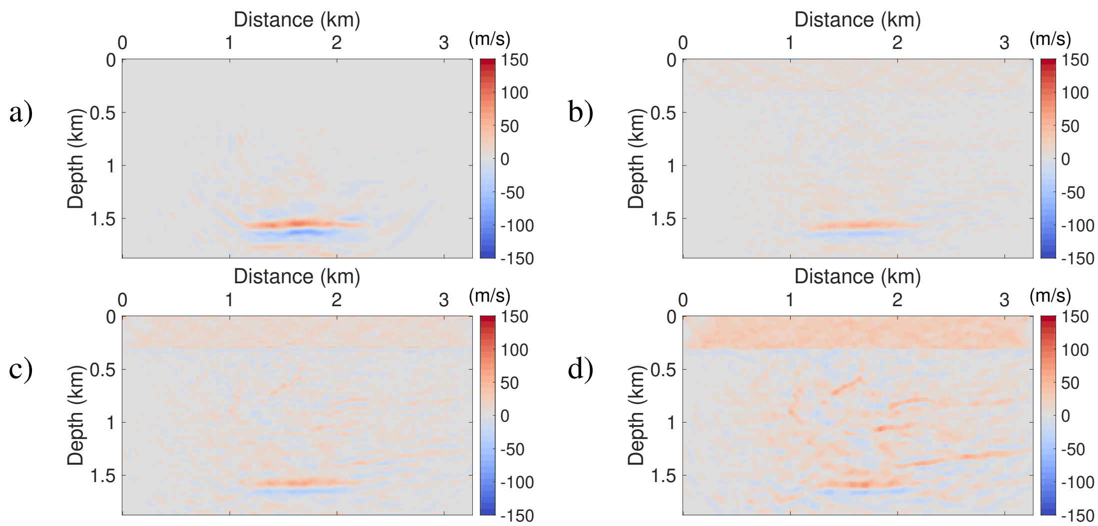

FIG. 5. Inverted time-lapse changes of the double-difference strategy, and the corresponding true time-lapse changes of (a), (b), (c), and (d) are, respectively, time-lapse changes 1 (Figure 4c), 2 (Figure 4d), 3 (Figure 4e), 4 (Figure 4f).

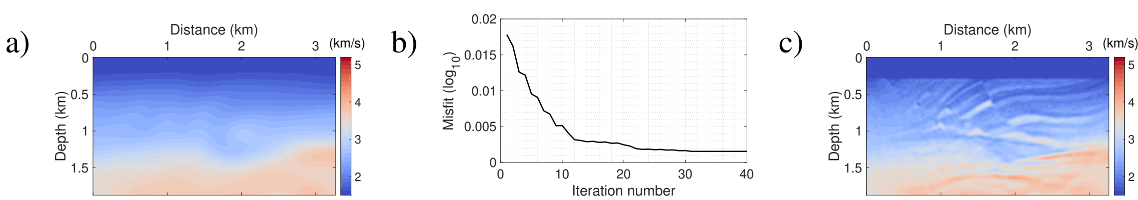

FIG. 6. The baseline inversion in stage 1 of the TSS. (a) Starting baseline model (i.e., $Starting\ model\ 1$ in Figure 2), (b) the curve of baseline data misfts versus iteration numbers, and (c) the inverted baseline model (i.e., $Baseline\ model\ 1$ in Figure 2).

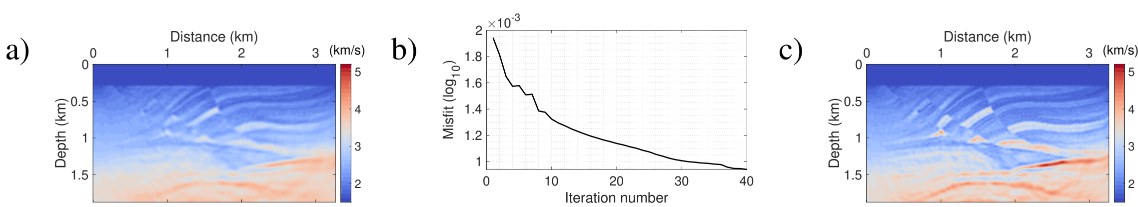

FIG. 7. The baseline inversion in stage 2 of the TSS. (a) Starting baseline model (i.e., $Baseline\ starting\ model\ 2$ in Figure 2), (b) the curve of baseline data misfts versus iteration numbers, and (c) the inverted baseline model (i.e., $Baseline\ model\ 2$ in Figure 2).

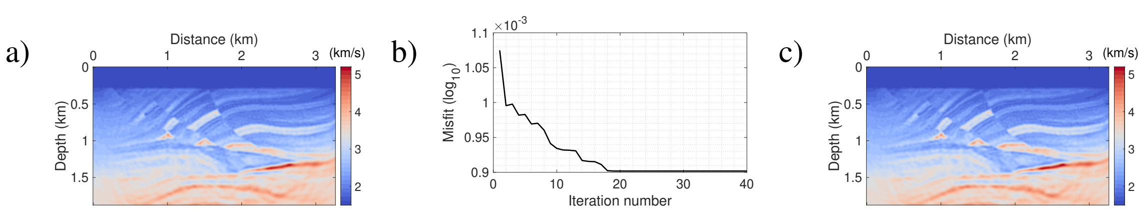

FIG. 8. The baseline inversion in stage 3 of the TSS. (a) Starting baseline model (i.e., $Baseline\ starting\ model\ 3$ in Figure 2), (b) the curve of baseline data misfts versus iteration numbers, and (c) the inverted baseline model (i.e., $Baseline\ model\ 3$ in Figure 2).

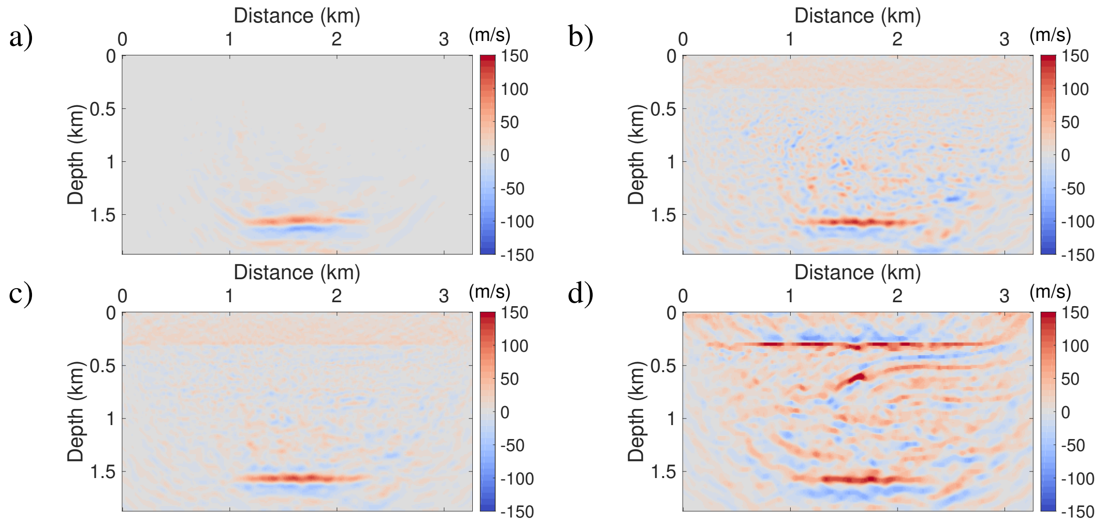

FIG. 9. Inverted time-lapse changes of the TTS, and the corresponding true time-lapse changes of (a), (b), (c), and (d) are, respectively, time-lapse changes 1 (Figure 4c), 2 (Figure 4d), 3 (Figure 4e), 4 (Figure 4f).

CONCLUSION

In this report, we have developed a three-stage time-lapse FWI strategy for OBN seismic data, in which the first stage is to use FWI to estimate the seawater velocities in the baseline model and the monitor model, respectively; the second stage is to obtain a relatively good common starting model that is close to the final inversion result, to guide the next baseline FWI and monitor FWI to converge to local minima that are closing to each other; the third stage is to employ the better starting models acquired in the second stage to carry out the final convergence and reflect the time-lapse differences. The tests using synthetic data obtained from acoustic models with different levels of seawater velocity changes have demonstrated the feasibility and stability of our new method.

ACKNOWLEDGEMENTS

We thank the sponsors of CREWES for continued support. This work was funded by CREWES industrial sponsors, NSERC (Natural Science and Engineering Research Council of Canada) through the grants CRDPJ 543578-19. Partial funding also came from the Canada First Research Excellence Fund.

REFERENCES

Ajo-Franklin, J., Peterson, J., Doetsch, J., and Daley, T., 2013, High-resolution characterization of a co2 plume using crosswell seismic tomography: Cranfield, ms, usa: International Journal of Greenhouse Gas Control, **18**, 497–509.

Asnaashari, A., Brossier, R., Garambois, S., Audebert, F., Thore, P., and Virieux, J., 2015, Time-lapse seismic imaging using regularized full-waveform inversion with a prior model: which strategy?: Geophysical prospecting, **63**, No. 1, 78–98.

Bortoni, S., Barragan, S., Azevedo, G., Cypriano, L., Ferreira, A., Moreira, W., dos Reis, P., and Filho, W., 2021, Learnings from an fwi imaging study using 3d and 4d data over a postsalt field in campos basin, *in* First International Meeting for Applied Geoscience & Energy, Society of Exploration Geophysicists, 587–591.

Byerley, G., Monk, D., Aaron, P., and Yates, M., 2018, Time-lapse seismic monitoring of individual hydraulic frac stages using a downhole das array: The Leading Edge, **37**, No. 11, 802–810.

Calvert, R., 2005, Insights and methods for 4D reservoir monitoring and characterization: Society of Exploration Geophysicists and European Association of ....

Cheng, A., Huang, L., and Rutledge, J., 2010, Time-lapse vsp data processing for monitoring co 2 injection: The Leading Edge, **29**, No. 2, 196–199.

Cho, Y., and Jun, H., 2021, Estimation and uncertainty analysis of the co2 storage volume in the sleipner field via 4d reversible-jump markov-chain monte carlo: Journal of Petroleum Science and Engineering, **200**, 108,333.

Egorov, A., Pevzner, R., Bóna, A., Glubokovskikh, S., Puzyrev, V., Tertyshnikov, K., and Gurevich, B., 2017, Time-lapse full waveform inversion of vertical seismic profile data: Workflow and application to the co2crc otway project: Geophysical Research Letters, **44**, No. 14, 7211–7218.

Fu, X., and Innanen, K. A., 2021, An mcmc-based approach to time-lapse full-waveform inversion, *in* First International Meeting for Applied Geoscience & Energy, Society of Exploration Geophysicists, 3484–3489.

Fu, X., and Innanen, K. A., 2022a, Stepsize sharing in time-lapse full-waveform inversion, *in* Second International Meeting for Applied Geoscience & Energy, Society of Exploration Geophysicists, 473–477.

Fu, X., and Innanen, K. A., 2022b, A time-domain, multi-source bayesian/markov chain monte carlo formulation of time-lapse seismic waveform inversion: Geophysics, **87**, No. 4, 1–110.

Fu, X., and Innanen, K. A., 2022c, Time-lapse seismic imaging using shot gathers with non-repeatable source wavelets: Geophysics, **88**, No. 1, 1–108.

Fu, X., Romahn, S., and Innanen, K., 2020, Double-wavelet double-difference time-lapse waveform inversion, *in* SEG Technical Program Expanded Abstracts 2020, Society of Exploration Geophysicists, 3764–3767.

Greaves, R. J., and Fulp, T. J., 1987, Three-dimensional seismic monitoring of an enhanced oil recovery process: Geophysics, **52**, No. 9, 1175–1187.

Hicks, E., Hoeber, H., Houbiers, M., Lescoffit, S. P., Ratcliffe, A., and Vinje, V., 2016, Time-lapse full-waveform inversion as a reservoir-monitoring tool—a north sea case study: The Leading Edge, **35**, No. 10, 850–858.

Huang, X., Jakobsen, M., Eikrem, K. S., and Nævdal, G., 2018, A target-oriented scheme for efficient inversion of time-lapse seismic waveform data, *in* 2018 SEG International Exposition and Annual Meeting, OnePetro.

Jack, I., 2017, 4d seismic—past, present, and future: The Leading Edge, **36**, No. 5, 386–392.

Kotsi, M., Malcolm, A., and Ely, G., 2020, Uncertainty quantification in time-lapse seismic imaging: a full-waveform approach: Geophysical Journal International, **222**, No. 2, 1245–1263.

Lailly, P., Bednar, J. et al., 1983, The seismic inverse problem as a sequence of before stack migrations: Conference on Inverse Scattering, Theory and Application, Society for Industrial and Applied Mathematics, Expanded Abstracts, 206–220.

Landrø, M., 2001, Discrimination between pressure and fluid saturation changes from time-lapse seismic data: Geophysics, **66**, No. 3, 836–844.

Li, Y., Alkhalifah, T., and Guo, Q., 2021, Target-oriented time-lapse waveform inversion using deep learning-assisted regularization: Geophysics, **86**, No. 4, R485–R495.

Lumley, D., Adams, D. C., Meadows, M., Cole, S., and Wright, R., 2003, 4d seismic data processing issues and examples, *in* SEG Technical Program Expanded Abstracts 2003, Society of Exploration Geophysicists, 1394–1397.

Lumley, D. E., 2001, Time-lapse seismic reservoir monitoring: Geophysics, **66**, No. 1, 50–53.

Macquet, M., Lawton, D. C., Saeedfar, A., and Osadetz, K. G., 2019, A feasibility study for detection thresholds of co2 at shallow depths at the cami field research station, newell county, alberta, canada: Petroleum Geoscience, **25**, No. 4, 509–518.

Maharramov, M., Biondi, B. L., and Meadows, M. A., 2016, Time-lapse inverse theory with applicationstime-lapse inverse theory: Geophysics, **81**, No. 6, R485–R501.

Medwin, H., 1975, Speed of sound in water: A simple equation for realistic parameters: The Journal of the Acoustical Society of America, **58**, No. 6, 1318–1319.

Plessix, R.-E., Michelet, S., Rynja, H., Kuehl, H., Perkins, C., de Maag, J., and Hatchell, P., 2010, Some 3d applications of full waveform inversion, *in* 72nd EAGE Conference and Exhibition-Workshops and Fieldtrips, European Association of Geoscientists & Engineers, cp–162.

Raknes, E. B., and Arntsen, B., 2014, Time-lapse full-waveform inversion of limited-offset seismic data using a local migration regularization: Geophysics, **79**, No. 3, WA117–WA128.

Rickett, J., and Lumley, D., 2001, Cross-equalization data processing for time-lapse seismic reservoir monitoring: A case study from the gulf of mexico: Geophysics, **66**, No. 4, 1015–1025.

Routh, P., Palacharla, G., Chikichev, I., and Lazaratos, S., 2012, Full wavefield inversion of time-lapse data for improved imaging and reservoir characterization, *in* SEG Technical Program Expanded Abstracts 2012, Society of Exploration Geophysicists, 1–6.

Shin, C., Jang, S., and Min, D.-J., 2001, Improved amplitude preservation for prestack depth migration by inverse scattering theory: Geophysical prospecting, **49**, No. 5, 592–606.

Shulakova, V., Pevzner, R., Dupuis, J. C., Urosevic, M., Tertyshnikov, K., Lumley, D. E., and Gurevich, B., 2015, Burying receivers for improved time-lapse seismic repeatability: Co2crc otway field experiment: Geophysical Prospecting, **63**, No. 1, 55–69.

Tarantola, A., 1984, Inversion of seismic reflection data in the acoustic approximation: Geophysics, **49**, No. 8, 1259–1266.

Virieux, J., and Operto, S., 2009, An overview of full-waveform inversion in exploration geophysics: Geophysics, **74**, No. 6, WCC1–WCC26.

Willemsen, B., Cao, J., and Roy, B., 2016, The impact of the acoustic approximation on time-lapse fwi, *in* 2016 SEG International Exposition and Annual Meeting, OnePetro.

Willemsen, L. A., 2017, Problems with a localized nature in exploration seismology: Ph.D. thesis, Massachusetts Institute of Technology.

Wilson, G. A., Willis, M. E., and Ellmauthaler, A., 2021, Evaluating 3d and 4d das vsp image quality of subsea carbon storage: The Leading Edge, **40**, No. 4, 261–266.

Yang, D., Liu, F., Morton, S., Malcolm, A., and Fehler, M., 2016, Time-lapse full-waveform inversion with ocean-bottom-cable data: Application on valhall field: Geophysics, **81**, No. 4, R225–R235.

Yang, D., Meadows, M., Inderwiesen, P., Landa, J., Malcolm, A., and Fehler, M., 2015, Double-difference waveform inversion: Feasibility and robustness study with pressure data: Geophysics, **80**, No. 6, M129–M141.

Zhang, Z., and Huang, L., 2013, Double-difference elastic-waveform inversion with prior information for time-lapse monitoring: Geophysics, **78**, No. 6, R259–R273.

Zheng, Y., Barton, P., and Singh, S., 2011, Strategies for elastic full waveform inversion of time-lapse ocean bottom cable (obc) seismic data, *in* SEG Technical Program Expanded Abstracts 2011, Society of Exploration Geophysicists, 4195–4200.

Zhou, W., and Lumley, D., 2021a, Central-difference time-lapse 4d seismic full-waveform inversion: Geophysics, **86**, No. 2, R161–R172.

Zhou, W., and Lumley, D., 2021b, Nonrepeatability effects on time-lapse 4d seismic full-waveform inversion for ocean-bottom node data: Geophysics, **86**, No. 4, R547–R561.

Zwartjes, P., Mateeva, A., Chalenski, D., Duan, Y., Kiyashchenko, D., and Lopez, J., 2018, Frequent, multi-well, stand-alone 3d das vsp for low-cost reservoir monitoring in deepwater, *in* SEG Technical Program Expanded Abstracts 2018, Society of Exploration Geophysicists, 4948–4952.